Characterization of Organosulfur Molecular Monolayers on Au(111) using Scanning Tunneling Microscopy

Gregory E. Poirier

National Institute of Standards and Technology, Gaithersburg, Maryland 20899

Contents

I. Introduction

In the early 1930s, amphiphile monolayers were used to control the wetting behavior of metal condenser plates in steam engines.[1-3] Wettability control was desired because dropwise condensation of steam resulted in >200% gains in heat conversion efficiency over filmwise condensation.[1] The explanation for this behavior is that when steam condenses as a uniform film, the film acts as a thermal barrier insulating the metal condenser plate from the ambient steam. In contrast, when steam condenses dropwise, the drops are removed from the plate by gravity, thereby exposing bare, cold condenser plate whereupon additional steam can condense.[3] Early researchers realized that drop condensation was due entirely to a monomolecular layer of amphiphilic molecules.[3] Further, they realized that these amphiphiles attach to the surface via metallophilic head groups and the hydrocarbon tails align with the surface normal forming a monolayer brush.[3] In a follow-up study in 1957, Blackman and Dewar compared the drop-condensation efficacy of a series of alkanethiols on copper.[4] Starting in the early 1980s, Nuzzo and Allara studied the related system of alkyl disulfide monolayers on gold surfaces.[5]

The early studies of amphiphile monolayers on metal surfaces were motivated by the desire to control wetting properties. In contrast, the recent efforts are motivated by potential applications in

chemical sensing,[6] biosensing,[7,8] biomimetics, and biocompatibility.[9,10] In parallel with alkanethiols on Au, a number of other organic monolayer systems have been developed and characterized. These include alkyltrichlorosilanes on SiO_2 and organic acids on mica or sapphire. Such systems belong to a class entitled "self-assembled monolayers". This review will not address all self-assembled monolayer systems but only those composed of thiol derivatized hydrocarbons [$HS(CH_2)_nX$; $0 \leq n \leq 21$, $X = CH_3$, OH, COOH, $c-C_6H_5$, etc., abbreviated C_nX] on Au(111) substrates (abbreviated AuC_nX).

AuC_nX has been studied using a plethora of analytical techniques and has been at least twice reviewed.[11,12] Of the techniques employed, scanning tunneling microscopy (STM) is unique in its ability to characterize structure, nondestructively, in direct space, and with routine single-molecule or single-atom resolution.[13,14] This review will not address all experimental and theoretical analyses, only those that employed STM to study AuC_nX.[15-89]

II. Alkanethiol Molecular Lattice

### a. Au(111) Herringbone Reconstruction

Au(111) is the lowest energy surface of gold, as reflected in the tendency of thin-film growth to propagate in the [111] direction.[90] Because technological applications of AuC_nX are more likely to rely on thin film Au, rather than single-crystal Au, most research efforts have focused on the Au(111) surface. The reconstructed surface of bare Au(111) (Figure 1A) is characterized by a 4.3% uniaxial lateral contraction relative to the bulk layers.[91] This contraction causes variations in registry between the surface and subsurface atomic layers such that the stacking arrangement alternates between normal *ABC* stacking and faulted *ABA* stacking with faulted and unfaulted regions delineated by rows of bridging Au atoms.[92] These bridging rows are manifest in STM topographs as elevated ridges aligned with substrate $\langle 1\bar{2}1 \rangle$ directions.[93] They pair, forming a $(\sqrt{3} \times 23)$ surface unit cell that can adopt one of three orientational registries. To further reduce surface energy the pairs form hyperdomains characterized by alternating 60° bends reminiscent of a herringbone pattern. Certain bend apices contain surface-confined dislocations and are more reactive surface sites.[93]

b. Early Monolayer Structure Studies

The forces that conspire to determine the structure of alkanethiol monolayers can be grouped into three classes: interactions between thiol head groups and the corrugated Au lattice, dispersion forces between the alkyl chains, and interactions between alkanethiol end groups. The balance of these forces determines the specific molecular packing habit. An early structure determination used electron diffraction and reported an incommensurate (7×7) molecular overlayer for $AuC_{21}CH_3$.[94] It was later reported that the correct interpretation of the Bragg reflections indicates a commensurate $(\sqrt{3} \times \sqrt{3})R30°$, which is a 30° rotation of the incommensurate (7×7).[95] Later infrared absorption (IR) studies confirmed that the monolayers are dense and solidlike. Moreover, IR showed that the thiols are tilted ~30° off of the surface normal and that the planes defined by the all-trans hydrocarbon backbone exist in two dissimilar twist azimuths.[96] Porter et al. were the first to report molecular resolution STM topographs of C_n-CH_3 on Au(111); their data showed a hexagonal lattice consistent with a $(\sqrt{3} \times \sqrt{3})R30°$.[73]

c. The c(4×2) Superlattice

In later studies, Camillone et al. reported He diffraction measurements that suggested an orthorhombic unit cell that comprises four thiols arranged as two like-pairs,[97] consistent with the IR data. The orthorhombic primitive unit cell reported in this study has dimensions of $3a \times 2\sqrt{3}a$ ($a = 2.884$ Å, the Au lattice constant) and can equally be described as a c(4×2) superlattice of a $(\sqrt{3} \times \sqrt{3})R30°$ hexagonal lattice. This structure was subsequently confirmed by grazing incidence X-ray diffraction (GIXD).[98] The c(4×2) superlattice was not reported in the initial STM study[73] but was seen in later studies that employed high-impedance tunneling junctions.[39,50,63]
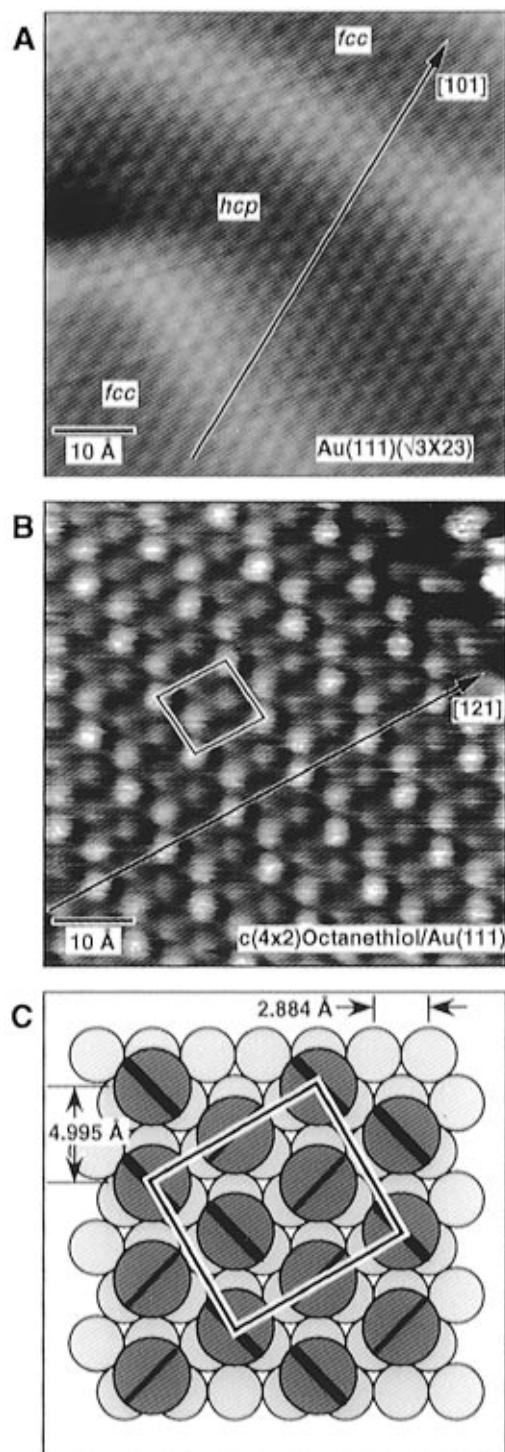
Figure 1. (A) Constant-current STM topograph of reconstructed Au(111) surface showing quasihexagonal arrangement of Au atoms and bright ridges due to variations in registry between surface and subsurface layers. Atomic rows deviate from linearity due to partial stacking fault in *hcp* regions (*ABA* stacking). (B) Constant-current STM topograph of octanethiol monolayer on Au(111). Au reconstruction is lifted and alkanethiols adopt commensurate crystalline lattice characteriized by a c(4×2) superlattice of a $(\sqrt{3} \times \sqrt{3})R30°$. (C) Model of commensuration condition between alkanethiol monolayer (large circles) and bulk-terminated Au surface (small circles). Diagonal slash in large circles represents azimuthal orientation of plane defined by all-trans hydrocarbon chain. (Part A: Reprinted from ref 118. Copyright 1992 Slack, Inc. Part B: Reprinted from ref 63. Copyright 1994 American Chemical Society.)

Figure 1B shows a molecular resolution image of an octanethiol monolayer on Au(111) with the rectangular primitive unit cell outlined. Each bright feature is attributed to an individual thiol molecule. The modulation in intensity reflects the presence of two discrete thiol conformations and their spatial arrangement agrees with the previous He diffraction[97] and X-ray diffraction measurements.[98] In addition to the spatial arrangement shown in Figure 1B, two other arrangements characterized by a c(4×2) superlattice and one characterized by a ($\sqrt{3}\times\sqrt{3}$)R30° primitive unit cell have been proposed to exist.[46,50,51] This suggestion of polymorphism, however, is contradicted by the absence in GIXD of certain reflections that are forbidden by the c(4×2) symmetry shown in Figure 1B, but are allowed by the proposed symmetries.[98,99] Interpretation of the internal structure of the unit cell is complicated by morphological limitations of STM.[100] "Convolution" of a cylindrically asymmetric tip with the various orientational and tilt domains can give the false impression of disparate internal structure. To date, polymorphism in AuC$_n$X has not been independently confirmed.

The two discrete molecular features comprising the unit cell were originally attributed to an alternation of the plane defined by the all-trans hydrocarbon backbones, a model consistent with the IR data (see Figure 1C).[96,97,101] Recently, Fenter et al. modeled GIXD truncation rod profiles. The modeling suggested that, in addition to alternation of the hydrocarbon backbones, neighboring sulfur atoms pair to form a surface disulfide.[99] Evidence in support of the surface disulfide model was reported in a subsequent study that employed resonant sum-frequency generation.[102]

III. Characterization of Defects

In the early stages of monolayer characterization, researchers were concerned about the degree of crystalline perfection of AuC$_n$X. The presence of disorder or pinholes could compromise the physical and electron-transfer blocking ability of the monolayers.[28–30] STM is capable of measuring local structure with atomic resolution and this makes it amenable to characterization of molecular and mesoscale defects in AuC$_n$X.

a. Domain Boundaries

The c(4×2) superlattice has a 3-fold orientational degeneracy, 12-fold positional degeneracy, and a 3-fold tilt degeneracy.[98] The low symmetry of the molecular lattice can give rise to various domain boundaries including tilt boundaries, stacking faults, rotational boundaries, and antiphase boundaries. Linebroadening in GIXD and He diffraction is able to provide an estimate of the average domain size;[98,103] however, direct-space imaging by STM is able to provide additional details such as domain shapes and size dispersion.[46,49,50,52,63,64,66,72,75,79,80,88] Figure 2A shows a large-area STM topograph of a AuC$_{11}$CH$_3$ surface. The Au(111) terraces are decorated by a tessellation of the various symmetry-equivalent rotational and translational domains. For this monolayer, the domain size ranges from 50 to 150 Å. Domain boundaries that are purely rotational can be infinitesimal twins, whereas domain boundaries with

a translational component display a finite width (see Figures 2, part B and C). Similar domain boundary networks are seen for the AuC$_n$X where X ≠ CH$_3$.[48,66,80]

b. Au Vacancy Islands

Examination of the domain boundary network of Figure 2A reveals that it is decorated by pitlike defects. These pit defects were first observed by Haussling et al.[53] Later work by Edinger et al. showed that the pit depth was 2.5 Å, consistent with the Au(111) single-atom step height, suggesting that the pits are defects in the Au surface layer, not defects in the alkanethiol layer.[33] Specifically, they were assigned to two-dimensional islands of Au vacancies.[33] The Au vacancy island model was later confirmed by numerous other STM studies.[40,41,43,49,64,65,77,78]

Edinger et al. proposed that the vacancy islands were formed by etching of Au in the alkanethiol solutions, a mechanism that was suggested by atomic absorption spectroscopy measurements showing dissolved Au species in the incubation bath.[33] This Au-etching mechanism was called into question by more recent experiments showing vacancy island formation during gas-phase assembly of C$_n$X.[28,67] A recent report suggested that the vacancy islands were formed by adsorbate-induced shrinkage of the surface lattice constant;[72] however, data existing in the literature indicate that the surface lattice constant is actually increased during monolayer assembly.[63,91,98] Recent work in our laboratory provided evidence for the existence of mobile Au-adatoms during monolayer assembly, suggesting that the vacancy islands form by ejection of excess Au atom density from the surface during relaxation of the Au(111) herringbone reconstruction.[69] At saturation monolayer coverage, the vacancy islands are uniformly covered by alkanethiols (see Figure 2A, inset), making them isomorphic with Au step edges.

The highly dispersed vacancy islands have a large perimeter-length-to-area ratio. Several studies have reported a coarsening of the vacancy island size distribution that is consistent with an Ostwald ripening process.[41,64,65] A distribution of particles undergoing Ostwald ripening is characterized by growth of large particles at the expense of small particles. Ripening of the vacancy island distribution is driven by a reduction in the total step-edge energy by reduction of the total edge length. Assuming vacancy, rather than adatom-mediated ripening, the mass transfer occurs by detachment of single-atom vacancies from the island edge, vacancy migration in the surface plane, and reattachment at another vacancy island. One study found that the rate of ripening is significantly enhanced when the monolayer is in a state of liquidlike disorder.[65] Several studies have shown that the coarsening of vacancy islands can be activated by invasive tunneling conditions,[16,40,43] and can be accelerated at elevated temperature.[40,43,49,52,70] Coarsening at elevated temperature may be enhanced due to melting of the monolayer above 350 K.[65,70,98] Two studies quantified the coarsening kinetics and found a power law time dependence.[41,65] The power law exponent was attributed to ripening kinetics dominated by attachment/detachment of single-atom vacancies.[41,42]
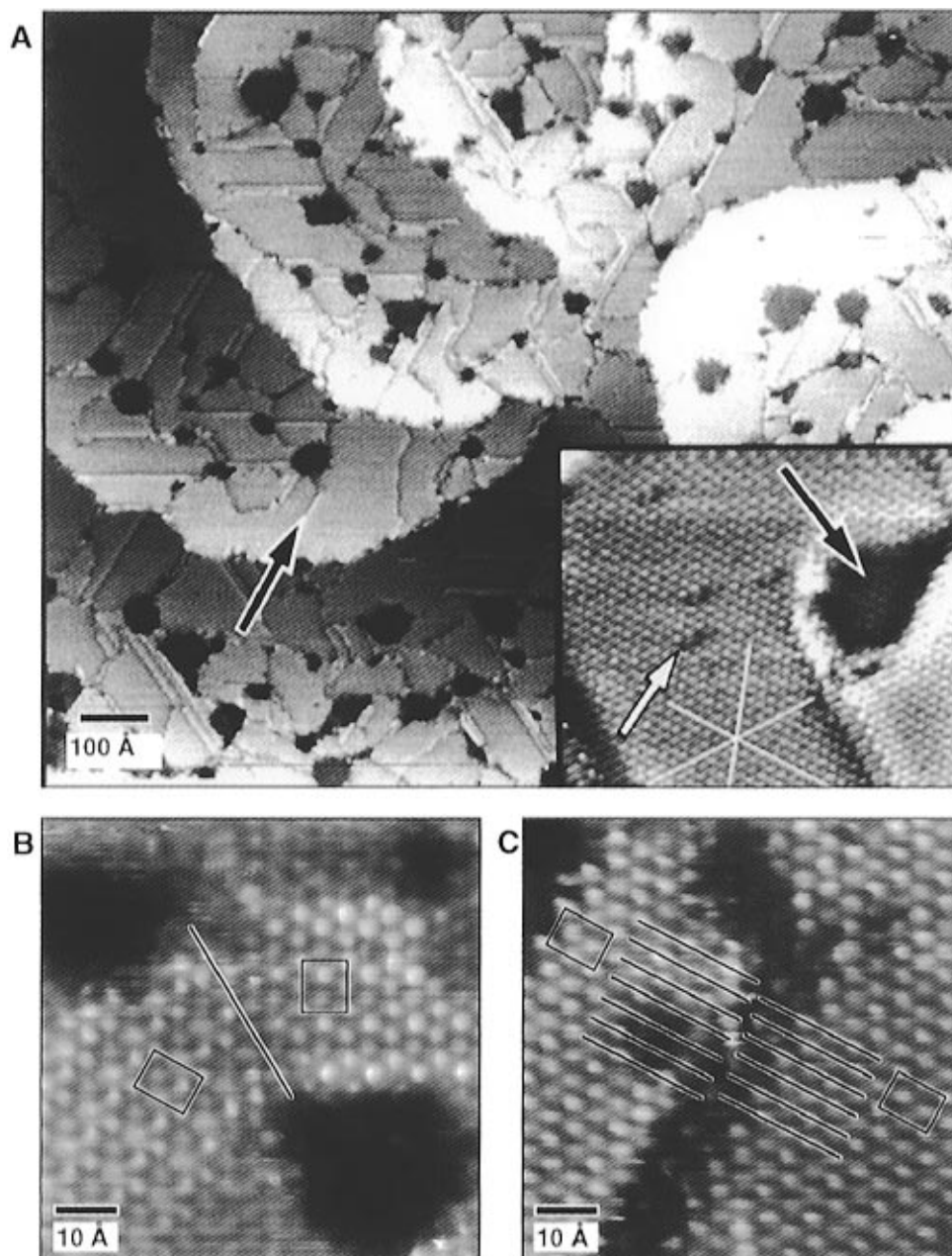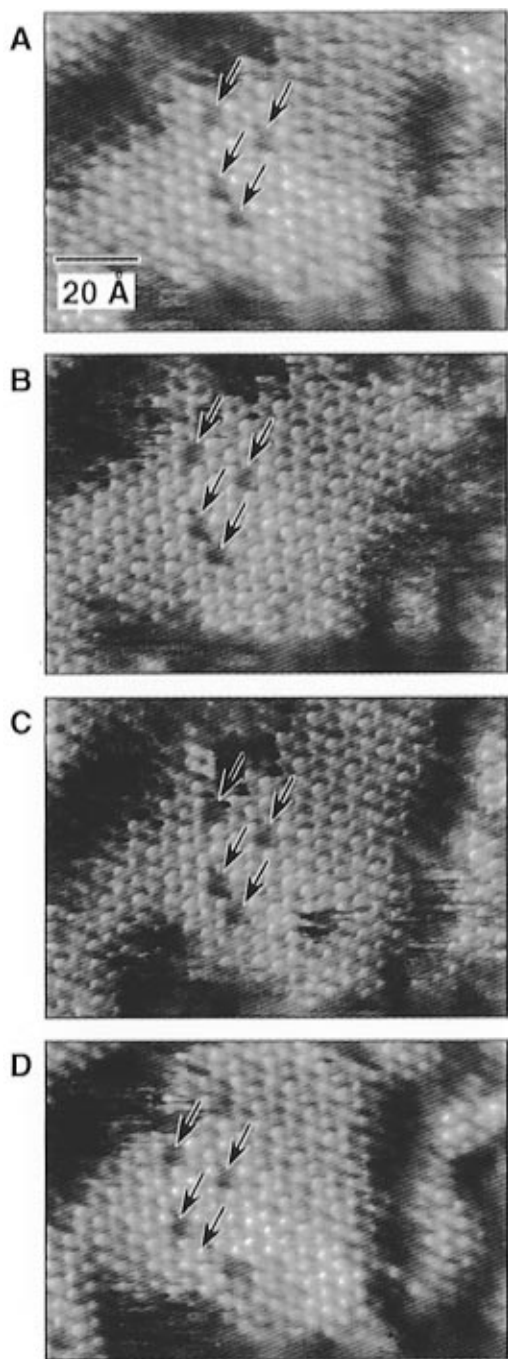
Figure 2. (A) Large area constant-current STM topograph of dodecanethiol monolayer on Au(111) showing mosaic of c(4×2) domains. Au terraces are separated by single atom steps. Domain boundaries are molecularly thin and are punctuated by vacancy islands. Inset shows molecular-resolution topograph of domain boundary. Molecular lattice is apparent in vacancy island (black arrow). (B) High-resolution constant-current STM topograph showing pure orientational domain boundary. Domain boundary is infinitesimal twin. (C) High resolution constant-current STM topograph showing pure translational domain boundary. Domain boundary has finite width. (Part A: Reprinted from ref 79. Copyright 1995 American Chemical Society. Part B: Reprinted from ref 63. Copyright 1994 American Chemical Society. Part C: G. E. Poirir, previously unpublished data.)

c. Molecular Vacancies

Commercial applications of alkanethiol monolayers may rely on spatially patterned mixed C_nX on Au. A critical parameter for mixed C_nX on Au is the rate of exchange diffusion or the rate of vacancy diffusion, because this determines the time scale over which the pattern will retain its integrity. The rate of vacancy diffusion can be addressed by deliberately creating isolated molecular vacancies and following their migration. Mild annealing in vacuum results in creation of isolated molecular vacancies in the alkanethiol surface lattice. Figure 3 shows a series of topographs of a decanethiol monolayer in which

four molecular vacancies were created by annealing to 325 K for 10 min. The relative positions of the arrow indicators is retained in the series of images. The first three images taken at ~2 min intervals show that, under the conditions of the experiment (10 pA, 300 mV_{sample}), the scanned probe does not induce vacancy motion. Following acquisition of the data Figure 3C, the tip was withdrawn, the bias voltage was zeroed, and the surface was allowed to evolve overnight. Figure 3D shows that one of the four vacancies migrated two molecular lattice sites overnight. Although the statistics are not good, this ensemble of four vacancies allows us to estimate the

Figure 3. Time series of constant-current STM topographs of decanethiol monolayer previously annealed in vacuum to 323 K for 10 min. Annealing results in desorption of a fraction of the alkanethiols thereby creating isolated vacancies in the molecular lattice (arrows). (A) Time $t = \tau$. (B) $t = \tau + 2$ min. (C) $t = \tau + 4$ min. (D) $t = \tau + 16$ h. Lower-right vacancy moves two lattice sites between frames C and D. (G. E. Poirier, previously unpublished data.)

vacancy diffusion coefficient for $AuC_{10}H$ at $\sim 1 \times 10^{-19}$ cm^2/s. This number is expected to depend on n and X.

IV. Variation of End Group and Chain Saturation

The surface physicochemical properties of dense alkanethiol monolayers are determined principally by the end group, X. The ability to customize surface properties by simply varying X is one aspect that makes AuC_nX so attractive. For example, by forming

monolayers from mixed composition solutions of C_n-CH_3 and C_mOH, one can continuously tune from extreme hydrophobicity to extreme hydrophylicity.[104,105] In addition, chain packing will influence the monolayer surface properties. It is important, therefore, to understand how substitutions of the end group will influence the molecular packing.

a. Alternate End Groups

Several research groups have used STM to explore the packing arrangement of AuC_nX with X $\neq$ CH_3.[15,31,37,38,48,51,52,57-60,66,74,80,88] Kim et al. were the first to report molecular-resolution STM topographs of alkanethiols terminated with bulky end groups, end groups for which $(\sqrt{3} \times \sqrt{3})R30°$ packing is sterically prohibited.[15] Results from this study suggested, nevertheless, that alkanethiols with bulky end groups exhibit a $(\sqrt{3} \times \sqrt{3})R30°$ lattice. The authors attributed this apparent anomaly to an STM contrast mechanism that is dominated by electron density of the Au surface.

This finding was refuted in a later study of monolayers of 6-[4-(phenylazo)phenoxy]hexane-1-thiol. This study resolved an incommensurate lattice with a primitive unit cell that encompassed an area of 48 Å^2.[48,51,52] If one assumes that the unit cell comprises two molecules, then the molecular area is 24 Å^2/molecule, an expansion of the 21.5 Å^2/molecule $(\sqrt{3} \times \sqrt{3})$-R30° packing. The reported molecular lattice is incommensurate; however, there was no evidence for the expected moire fringes. Expanded lattices were confirmed in other STM studies of monolayers composed of alkanethiols with bulky end groups.[37,38,60] The earlier study by Kim et al. employed low gap impedances (5-400 MΩ), relative to the later study (which employed ~500 GΩ), and this may explain the disparity in results. Gap impedances on the order of gigaohms are required to image extended amphiphile monolayers in a low-perturbation mode.[50,63,79]

Monolayers composed of alkanethiols with end groups such as X = OH or NH$_2$ have technological importance in applications such as control of ionic binding,[106] in preparation of covalent multilayer films,[107] and in studies of biocompatibility and wetting.[10,105,108-110] Consequently, there is much interest in whether these form dense, ordered monolayers. The OH and NH$_2$ end groups are nonbulky; therefore, the $(\sqrt{3} \times \sqrt{3})R30°$ lattice is sterically allowed. Sprik and co-workers studied $AuC_{11}OH$ and $AuC_{12}NH_2$ monolayers prepared by incubating Au in ethanol solutions of the respective alkanethiols. Their results showed ordered structures; however, conclusive packing assignments were hindered by contamination of the monolayers.[58] The contamination issue was resolved in a later study that employed vapor transport of C_6OH onto Au(111) in ultrahigh vacuum.[66] The later study indicated that these monolayers exhibit a packing habit with the same molecular area as AuC_nCH_3 (21.5 Å^2/molecule) but the presence of the hydroxyl end group induces a distortion from an orthorhombic to an oblique primitive unit cell (see Figure 4).[66] It was further observed that exposure of the pristine hydrophilic surfaces to water vapor resulted in significant structural changes.[66] The studies outlined in this and the previous paragraph show that both steric and chemical
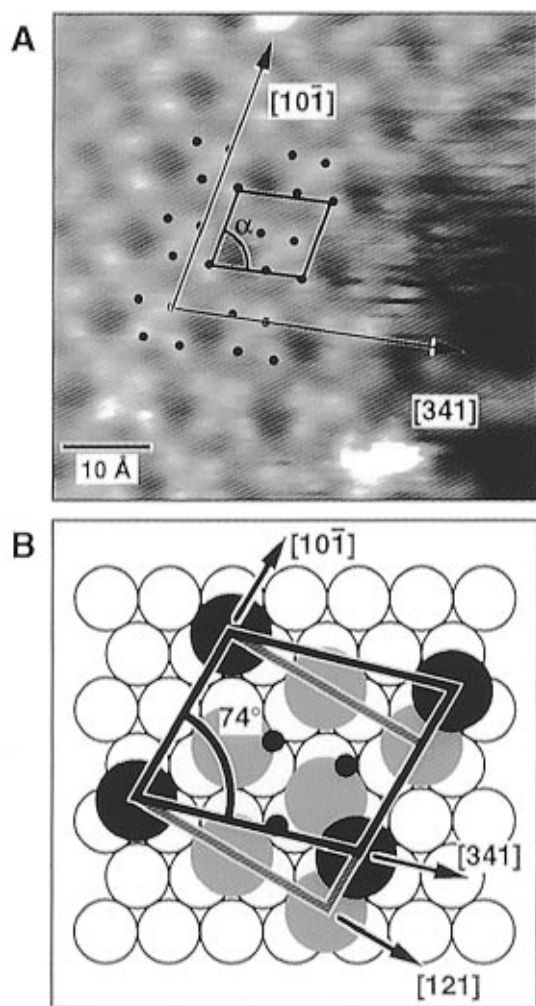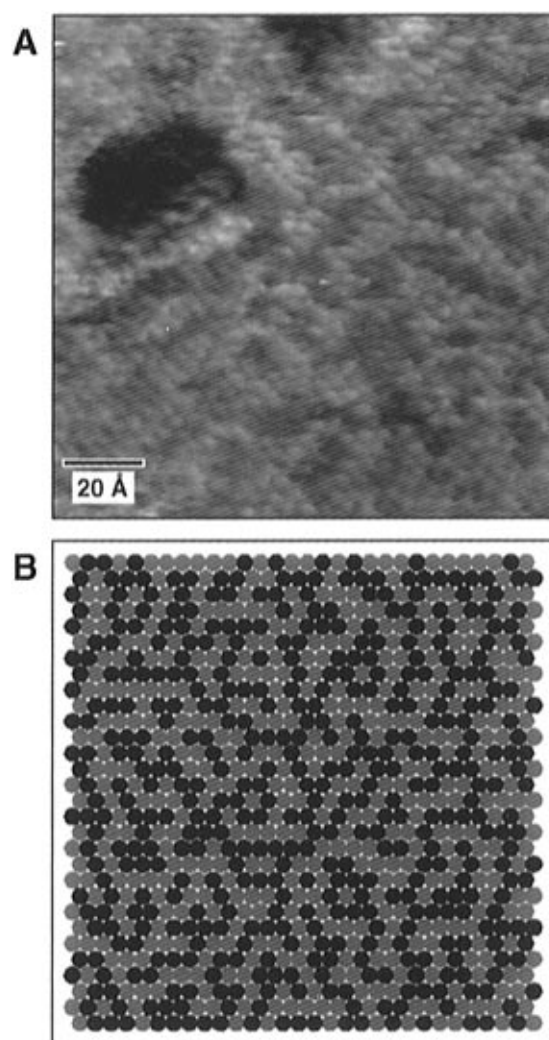
Figure 4. (A) Constant-current STM topograph showing the commensurate crystalline packing arrangement of pristine mercaptohexanol monolayer on Au(111) in ultra-high vacuum. The primitive unit-cell is oblique and has dimensions of $a = 3a$, $b = \sqrt{13}a$; a = 2.88 Å, the Au lattice constant, $\alpha = \arctan(2\sqrt{3}) \approx 74°$. (B) Schematic of the oblique primitive unit cell of mercaptohexanol on Au(111) (black parallelogram) and the orthorhombic cell of methyl-terminated monolayers (gray rectangle). Large black circles represent oblique cell corner molecules, small black circles represent oblique cell center molecules, large gray circles represent packing for methyl-terminated homologues. (Reprinted from ref 66. Copyright 1996 America Institute of Physics.)

bonding interactions can alter the AuC$_n$X molecular lattice.

b. Nonaliphatic Monolayers

Dhirani and co-workers addressed the question of whether thiol-based amphiphiles with nonaliphatic hydrocarbon chains would still form dense, physically blocking monolayers. They chose monolayers composed of rigid-rod molecules for which the all-trans hydrocarbon backbone is replaced by acetylene-linked phenyl rings. The van der Waals cross section of these molecules is small enough to accommodate a $(\sqrt{3}\times\sqrt{3})$R30° packing arrangement if the rigid-rod molecular long axes align with the surface normal. The results indicate that the linked-phenyl thiols adopt a $(\sqrt{3}\times\sqrt{3})$R30°-based commensurate lattice similar to that of saturated linear chain thiols.[80]

Figure 5. (A) Constant-current STM topograph of monolayer of $CH_3(CH_2)_{11}SS(CH_2)_{11}OH$ on Au(111). Dark and light molecular features are hexagonally packed, appear in equal numbers, and are attributed to inequivalent halves of the asymmetric disulfide. Dark features are vacancy islands. Tunneling parameters are 0.9 V_{sample}, 5 pA. (B) Pattern generated by placing asymmetric dimers on hexagonal lattice with random selection of symmetry-equivalent dimer azimuths. (Reprinted from ref 57. Copyright 1995 American Chemical Society.)

These results are important because they establish that, in addition to controllable surface physicochemical properties, it is possible to form organized monolayers that have controllable electron-transfer properties.[81]

c. Mixed Monolayers

Technological applications of AuC$_n$X systems may rely on mixed monolayers that comprise two or more C$_n$X of differing n or X.[51,52,57,88] A mixed composition monolayer can form a homogeneous two-dimensional alloy, or can decompose into a heterogeneous distribution of chemically distinct domains, depending on the balance of forces. Takami et al. performed experiments on monolayers of asymmetric disulfides of the form X$_1$(CH$_2$)$_{n_1}$SS(CH$_2$)$_{n_2}$X$_2$; where $n_1 = n_2 = 11$, X$_1$ = CH$_3$, and X$_2$ = OH.[57] STM topographs show two feature types of differing apparent height, packed in a hexagonal lattice (see Figure 5A). The two
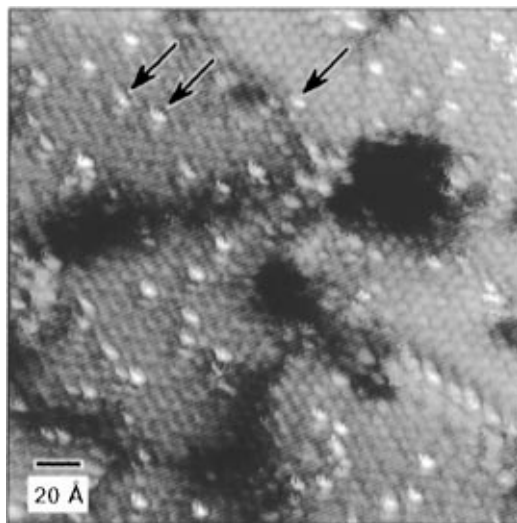
Figure 6. Constant-current STM topograph of monolayer formed by incubating Au(111) in 5% dodecanethiol, 95% decanethiol (1×10^{-3} mol/L total alkanethiol concentration in ethanol). Number density of bright features, indicated by arrows, is consistent with assignment as individual dodecanethiol molecules in c(4×2) decanethiol matrix. (Data courtesy of L. A. Bumm, Pennsylvania State University.)

feature types are reported to exist in equal numbers. Each feature in the lattice has at least one nearest neighbor of the opposite type, indicating that either there is no strong driving force for phase separation, or that the kinetics of such a phase separation are slow on the time scale of the measurement (minutes). Figure 5B shows a model surface created by placing randomly oriented asymmetric dimers in a hexagonal lattice; it shows qualitative consistency with the experimental result. Imaging such monolayers in air is problematic because half of the end groups are hydrophilic.

Bumm and co-workers examined monolayers that comprise C_9CH_3 and $C_{11}CH_3$. The monolayers were formed by incubating Au(111) in ethanol-solvated mixtures of both molecules. The assembly dynamics of long-chain alkanethiols are known to be faster than those of short-chain alkanethiols;[111] however, because the two molecules in this study are of comparable length, the fractional surface concentration is expected to reflect that in solution. For the case of $[C_{11}CH_3]:[C_9CH_3] = 0.05:0.95$, Figure 6 shows a c($4\times2$) lattice of the major component decorated by isolated protrusions that are attributed to the minor component. The data described in this and in the previous paragraph show that the STM contrast mechanism for AuC_nX monolayers is sensitive to both X and n and, therefore, that STM is amenable to addressing questions about diffusion, phase separation, and alloy formation in mixed monolayers.

Bumm and co-workers performed related experiments on monolayers that comprise both aliphatic and aromatic thiols. They first formed AuC_9CH_3 monolayers and subsequently incubated in ethanol solutions of a fully conjugated molecule, oligo(phenylethynyl)benzenethiol.[88] The second incubation step results in a distribution of bright features localized in domain boundaries of the C_9CH_3 monolayer (see Figure 7). These data suggest that exchange can be
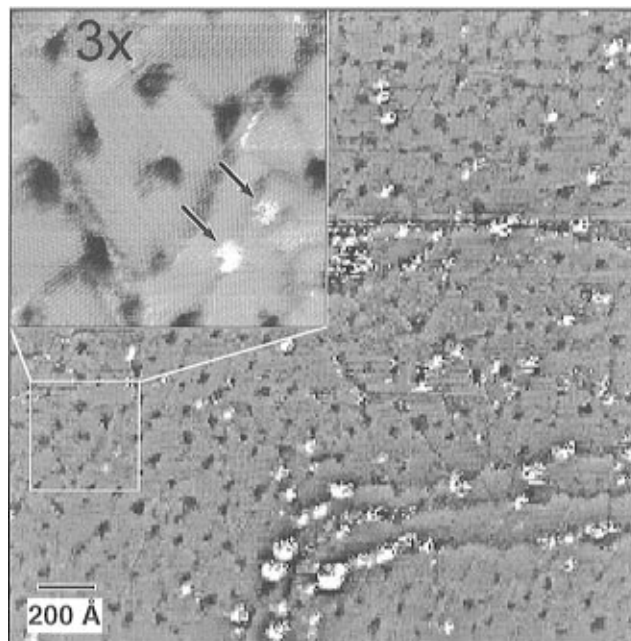
Figure 7. Constant-current STM topograph of decanethiol monolayer substitution doped with fully conjugated linked-phenyl arylthiol molecule. Bright features are attributed to individual linked-phenyl monomers. High-resolution scan (inset) suggest that aryl thiols preferentially insert in decanethiol domain boundaries. (Reprinted from ref **88**. Copyright 1996 American Association for the Advancement of Science.)

mediated by domain boundary defects for mixed monolayers prepared using a displacement strategy.

V. Variation of Coverage

The surface coverage of alkanethiols can be varied in one of two ways, by controlled deposition on a bare surface or by thermal desorption from a complete monolayer. The next two sections address both mechanisms of variation of surface coverage.

a. Assembly Mechanism

The growth kinetics of AuC_nX have been studied using ellipsometry and contact angle measurements,[112] surface acoustic wave devices,[113] second-harmonic generation,[114] and quartz crystal microbalances.[115] These studies found that the growth rate is proportional to the number of unoccupied adsorption sites, in agreement with simple first-order Langmuir adsorption kinetics.[113–115] A later study employed STM to answer questions about the microscopic aspects of monolayer assembly.[67] The STM study used gas-phase transport of neat alkanethiols onto Au(111) in ultrahigh vacuum. Figure 8, parts A–D, show a series of STM topographs acquired at increasing coverage of C_6OH. Each frame was acquired in nominally the same surface region with a frame-to-frame lateral image drift of less than 100 Å. Low exposures of C_6OH result in the appearance of islands exhibiting a striped pattern (Figure 8B). The stripes are aligned with substrate $\langle 1\overline{2}1 \rangle$ directions, exhibit a corrugation period of 5 Å along the row, and exhibit an interrow spacing of 22 Å.[67] These features are attributed to islands of alkanethiols, sulfur atoms bound in next-nearest-neighbor three-fold hollow
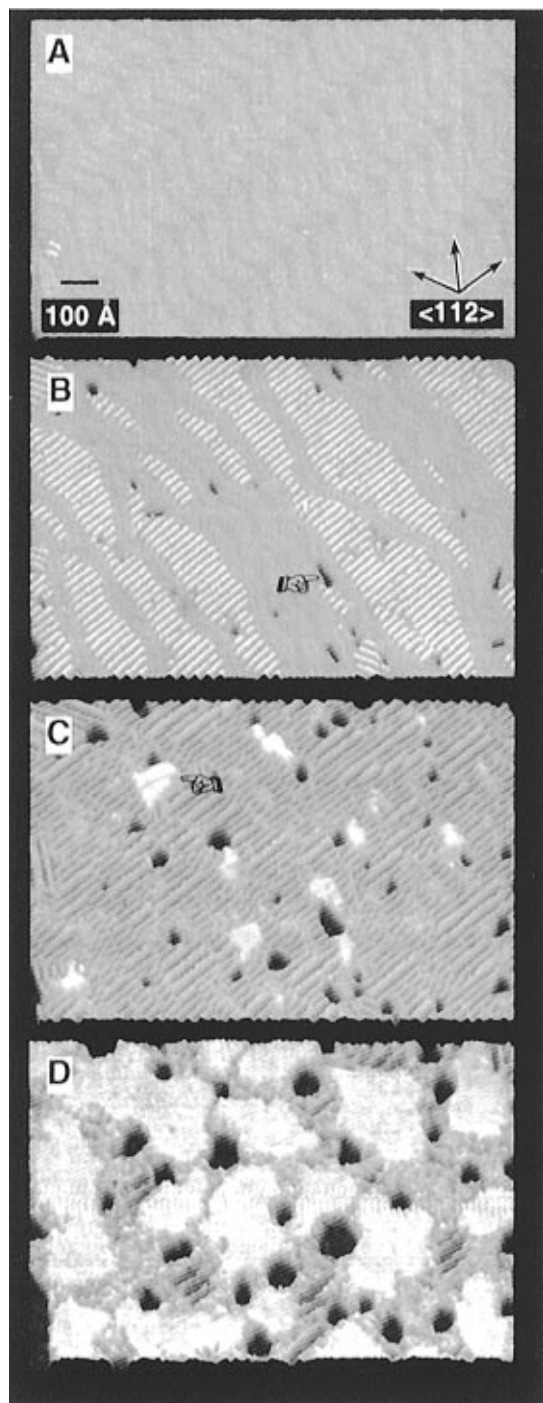
Figure 8. STM constant-current topographs showing evolution of the reconstructed Au(111) surface during gas-phase deposition of mercaptohexanol. (A) Nominally bare surface exhibits herringbone reconstruction. (B) Surface-aligned phase of mercaptohexanol (striped islands) grow after 600 Langmuirs exposure. Concomitant with mono-layer growth, vacancy islands nucleate and grow at her-ringbone elbows (pointing finger). (C) After 1000 Lang-muirs exposure, just above saturation of striped phase, surface undergoes first-order, solid−solid phase transition by heterogeneous nucleation of surface normal aligned phase (pointing finger). (D) Surface normal aligned phase grows at expense of striped phase until saturation. (Re-printed from ref 67. Copyright 1996 American Association for the Advancement of Science.)

sites, and molecular axes aligned with the surface plane. The STM topographs do not constitute un-ambiguous proof; however, support for this model is

found in recent helium diffraction measurements which show a correlation between interrow stripe period and alkanethiol chain length.[116] The Au vacancy island defects, discussed in section III.b, are seen to nucleate at herringbone elbows (pointing finger, Figure 8B). Continued exposure of the surface to C_6OH vapor results in complete saturation of the surface-aligned phase. Just above saturation, el-evated, corrugated islands appear (pointing finger, Figure 8C). These are attributed to islands of dens-est packed alkanethiol in which the molecular axes are directed along the surface normal. The appear-ance of discrete surface-aligned and surface normal-aligned phases is suggestive of a first-order phase transition. Under continued surface flux, these dense islands grow laterally and finally coalesce with formation of a domain boundary network, as dis-cussed in section III.a. These studies demonstrate that STM may be used to directly probe molecular scale aspects of monolayer structure during growth.

b. Thermal Decomposition Mechanism

Potential technical applications of AuC_nX include chemical sensing[6] and surface passivation,[28−30] ap-plications for which thermal and temporal stability are desirable. Annealing results in excitation of chemical bonds; excitation of the S−Au bond can result in molecular desorption, excitation of the S−C bond can result in surface decomposition. Several STM studies have explored the temperature stability and thermal decomposition pathway of AuC_n-X.[40,41,43,49,51,52,68,70] The STM data suggest that AuC_nX can be annealed to 325 K with no major structural changes, except for a coarsening of the domain boundary network and a ripening of the vacancy island distribution.[40,41,43,49,70] These changes are both driven by edge-tension. The domain boundaries migrate under the influence of their own curvature.[117] The vacancy islands coarsen by Ostwald ripening, rather than by diffusion and coalescence.[41,65] For long anneal times, the vacancy islands disappear due to transfer of vacancies to macroscopic (very low curvature) step edges.

Monolayers annealed above 350 K exhibit signifi-cant structural changes.[49,51,52,70,98] The mechanism of monolayer decomposition depends on whether the monolayer is annealed in vacuum,[70] or in air.[49,51,52] Samples annealed in vacuum appear to undergo a melting transition above 350 K that is accompanied by disappearance of the vacancy islands and desorp-tion of a fraction of the surface thiols (see Figure 9, parts A−C). Quenching to room temperature recrys-tallizes the monolayer into a structure that comprises high- and low-density domains in relative fractions determined by the total remnant surface coverage. Figure 9B displays phase coexistence similar to Figure 8C,D. Annealing samples above 575 K results in reappearance of the Au herringbone reconstruction suggesting complete desorption of the alkanethiol monolayer (see Figure 9C). In contrast, air annealing at 375 K for 20 h results in desorption of surface thiols and creation of missing row defects (see Figure 9, parts D−F). Continued annealing results in the appearance of disordered regions that are attributed to oxidized thiols, subsequent desorption of these sulfonates, and retention of a carbonaceous contami-
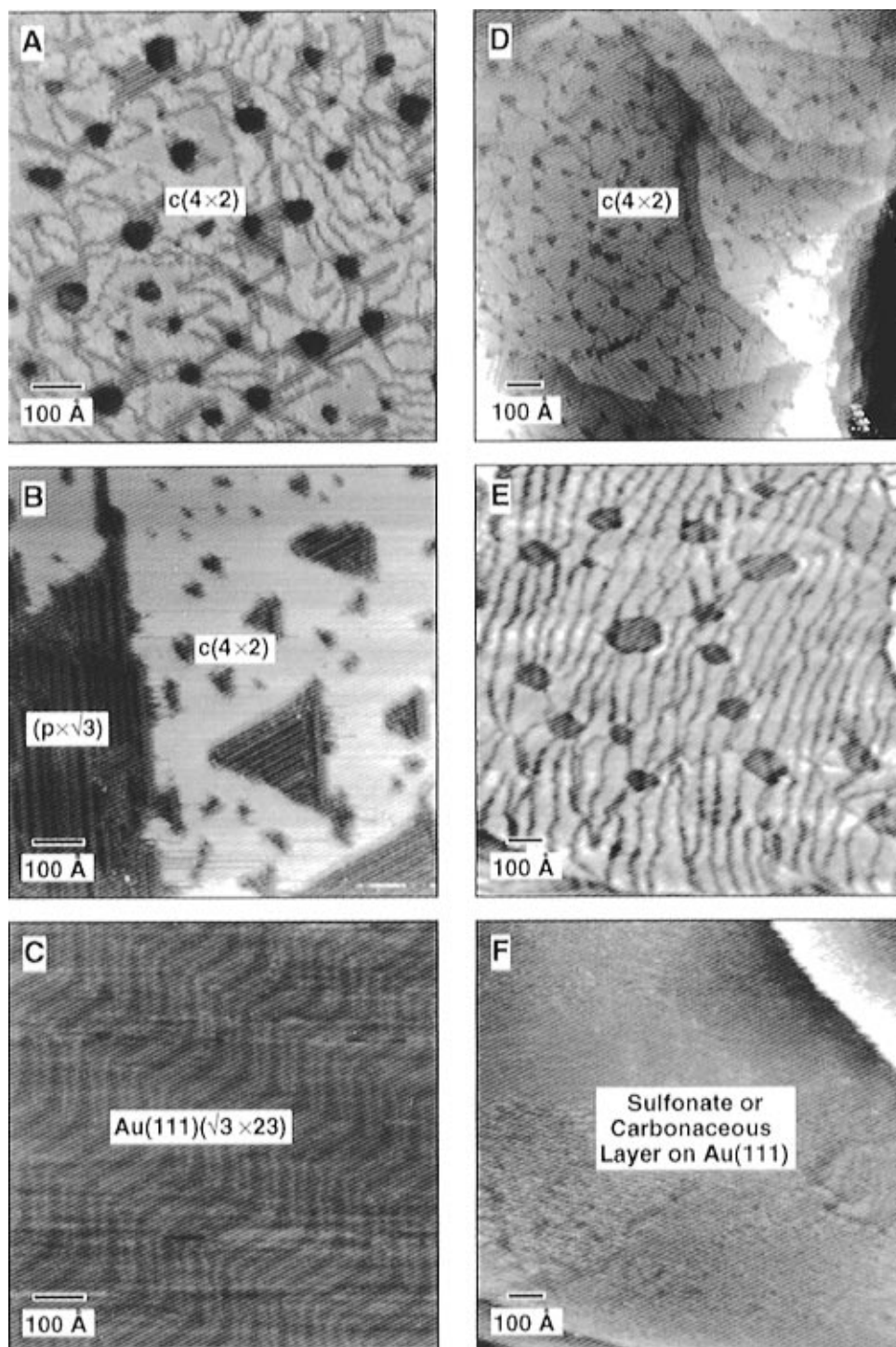
Figure 9. Constant-current STM topographs showing evolution of alkanethiol monolayer structure during annealing in vacuum (A)−(C), and in air (D)−(F). Both monolayers were deposited from ethanol solution and all images were acquired at 300 K. (A) Decanethiol monolayer deposited at 300 K and annealed to 325 K for 5 min in vacuum. Surface exhibits c(4×2) domains, domain boundary network, and vacancy islands. (B) Monolayer as in A, annealed to 375 K for 10 min in vacuum. Surface exhibits large c(4×2) domains and large domains of the lower density (p×√3) phase. (C) Monolayer as in B, annealed to 575 K for 10 min in vacuum. Surface exhibits herringbone reconstruction characteristic of clean Au-(111). (D) Dodecanethiol monolayer deposited at 325 K. Surface exhibits c(4×2) domains, domain boundary network, vacancy islands, and single atom Au steps. (E) Monolayer as in D, annealed to 375 K for 2 h in air. Vacancy islands have coarsened and dark stripes, attributed to missing thiol rows, are created. (F) Monolayer as in E, annealed to 375 K for 40 h in air. Surface exhibits dense stripes and disordered regions. These features are attributed to either surface sulfonates or residual surface carbon. (Parts A−C: Reprinted from ref 70. Copyright 1994. American Institute of Physics. Parts D−F: Reprinted from ref 49. Copyright 1994 American Chemical Society.)

nation layer (see Figure 9F).[49] The proposed sequence of events for air-annealed samples is supported by X-ray photoelectron spectroscopy (XPS) studies that show oxygen 1s photoemission at intermediate anneal times and subsequent disappearance of the oxygen feature with retention of a carbon 1s feature.[49] These two studies suggest that annealing in vacuum results in molecular desorption of intact alkanethiols, whereas annealing in air results in decomposition on the surface.

VI. Summary

Many complementary structural characterizations of AuC_nX have been conducted prior to, and in parallel with, the STM studies outlined in this review. The STM studies, however, are unique because they routinely resolve molecular-scale crystalline, noncrystalline, and defect structures in real space. The major revolution in STM of AuC_nX came with the realization that molecular resolution could be attained in a noninvasive fashion by using high gap impedances (>10 GΩ) and by using relatively short alkanethiol monomers ($n < 16$). Several questions remain with regard to STM characterization of the AuC_nX. These include the precise mechanism of image contrast, the exact identity of the electronic states that contribute to the tunneling current, and the conditions that lead to phase separation in mixed monolayers. Answers to these questions are all within reach using current experimental and theoretical tools, and they will likely be resolved in coming months or years.

VII. Acknowledgments

By promptly and generously responding to my requests for figures, for information, and for advice, Lloyd Bumm, Emmanuel Delamarche, Paul Fenter, Christian Schonenberger, and Joseph Stroscio greatly assisted the successful compilation of this review article.

VIII. References

(1) Schmidt, E.; Schurig, W.; Sellschopp, W. *Tech. Mech. Thermodyn.* **1930**, *1*, 53.
(2) Nagle, W. M.; Drew, T. B. *Trans. Am. Inst. Chem. Eng.* **1933**, *30*, 217.
(3) Emmons, H. *Trans. Am. Inst. Chem. Eng.* **1939**, *35*, 109.
(4) Blackman, L. C. F.; Dewar, M. J. S. *J. Chem. Soc.* **1957**, 162.
(5) Nuzzo, R. G.; Allara, D. L. *J. Am. Chem. Soc.* **1983**, *105*, 4481.
(6) Ricco, A. J.; Kepley, L. J.; Thomas, R. C.; Sun, L.; Crooks, R. M. *Technical Digest Series*; IEEE Solid-State Sensor and Actuator Workshop, Hilton Head Island SC; IEEE: Piscataway, NJ, 1992, 114.
(7) Haussling, L.; Knoll, W.; Ringsdorf, H.; Schmitt, F.-J.; Yang, J. *Makromol. Chem., Macromol. Symp.* **1991**, *46*, 145.
(8) Pevzner, P. A.; Lipshutz, R. J. *Proceedings of Mathematical Foundations of Computer Science*, 19th International Symposium, Kosice, Slovakia; Springer-Verlag: Berlin, Germany, 1994, p 143.
(9) Prime, K. L.; Whitesides, G. M. *J. Am. Chem. Soc.* **1993**, *115*, 10714.
(10) DiMilla, P. A.; et al. *J. Am. Chem. Soc.* **1994**, *116*, 2225.
(11) Ulman, A. *Chem. Rev.* **1996**, *96*, 1533.
(12) Dubois, L. H.; Nuzzo, R. G. *Annu. Rev. Phys. Chem.* **1992**, *43*, 437.
(13) Binnig, G.; Rohrer, H.; Gerber, C.; Weibel, E. *Appl. Phys. Lett.* **1982**, *40*, 178.
(14) Binnig, G.; Rohrer, H. *Helv. Phys. Acta.* **1982**, *55*, 726.
(15) Kim, Y.-T.; McCarley, R. L.; Bard, A. J. *J. Phys. Chem.* **1992**, *96*, 7416.
(16) Kim, Y.-T.; Bard, A. J. *Langmuir* **1992**, *8*, 1096.
(17) Kim, Y.-T.; McCarley, R. L.; Bard, A. J. *Langmuir* **1993**, *9*, 1941.
(18) McCarley, R. L.; Kim, Y.-T.; Bard, A. J. *J. Phys. Chem.* **1993**, *97*, 211.
(19) Ogawa, S.; Fan, F.-R.; Bard, A. J. *J. Phys. Chem.* **1995**, *99*, 11182.
(20) Han, T.; Beebe, T. B. *Langmuir* **1994**, *10*, 2705.
(21) Lercel, M. J.; Redinbo, G. F.; Craighead, H. G.; Sheen, C. W.; Allara, D. L. *Appl. Phys. Lett.* **1994**, *65*, 974.
(22) Sun, L.; Crooks, R. M. *J. Electrochem. Soc.* **1991**, *138*, L23.
(23) Sun, L.; Crooks, R. M. *Langmuir* **1993**, *9*, 1951.
(24) Corbitt, T. S.; Crooks, R. M.; Ross, C. B.; Hampden-Smith, M. J.; Shoer, J. K. *Adv. Mater.* **1993**, *5*, 935.
(25) Ross, C. B.; Sun, L.; Crooks, R. M. *Langmuir* **1993**, *9*, 632.
(26) Schoer, J. K.; Ross, C. B.; Crooks, R. M.; Corbitt, T. S.; Hampden-Smith, M. J. *Langmuir* **1994**, *10*, 615.
(27) Schoer, J. K.; Zamborini, F. P.; Crooks, R. M. *J. Phys. Chem.* **1996**, *100*, 11086.
(28) Chailapakul, O.; Sun, L.; Xu, C.; Crooks, R. M. *J. Am. Chem. Soc.* **1993**, *115*, 12459.
(29) Zamborini, F. P.; Crooks, R. M. *Langmuir* **1997**, *13*, 122.
(30) Li, Y.-Q.; Chailapakul, O.; Crooks, R. M. *J. Vac. Sci. Technol. B.* **1995**, *13*, 1300.
(31) Dishner, M. H.; Hemminger, J. C.; Feher, F. J. *Langmuir* **1996**, *12*, 6176.
(32) Dishner, M. H.; Feher, F. J.; Hemminger, J. C. *Chem. Commun.* **1996**, 1971.
(33) Edinger, K.; Golzhauser, A.; Demota, K.; Woll, C.; Grunze, M. *Langmuir* **1993**, *9*, 4.
(34) Grunze, M. *Phys. Scr.* **1993**, *T49B*, 711.
(35) Hallmark, V. M.; Leone, A.; Chiang, S.; Swalen, J. D.; Rabolt, J. F. *Mikrochim. Acta* **1988**, *11*, 39.
(36) Hara, M.; Sasabe, H.; Knoll, W. *Thin Solid Films* **1996**, *273*, 66.
(37) Katsumata, S.; Ide, A. *Jpn. J. Appl. Phys.* **1994**, *33*, 3723.
(38) Katsumata, S.; Ide, A. *Jpn. J. Appl. Phys.* **1995**, *34*, 3360.
(39) Bucher, J.-P.; Santesson, L.; Kern, K. *Appl. Phys. A* **1994**, *59*, 135.
(40) Bucher, J.-P.; Santesson, L.; Kern, K. *Langmuir* **1994**, *10*, 979.
(41) Cavalleri, O.; Hirstein, A.; Kern, K. *Surf. Sci.* **1995**, *340*, L960.
(42) Cavalleri, O.; Hirstein, A.; Bucher, J.-P.; Kern, K. *Thin Solid Films* **1996**, *284−285*, 392.
(43) McCarley, R. L.; Dunaway, D. J.; Willicut, R. J. *Langmuir* **1993**, *9*, 2775.
(44) Willicut, R. J.; McCarley, R. L. *Anal. Chim. Acta* **1995**, *307*, 269.
(45) Anselmetti, D.; et al. *Europhys. Lett.* **1993**, *23*, 421.
(46) Anselmetti, D.; et al. *Europhys. Lett.* **1994**, *27*, 365.
(47) Anselmetti, D.; et al. *J. Vac. Sci. Technol. B* **1994**, *12*, 1677.
(48) Wolf, H.; et al. *J. Phys. Chem.* **1995**, *99*, 7102.
(49) Delamarche, E.; Michel, B.; Kang, H.; Gerber, C. *Langmuir* **1994**, *10*, 4103.
(50) Delamarche, E.; et al. *Langmuir* **1994**, *10*, 2869.
(51) Delamarche, E.; Michel, B.; Biebuyck, H. A.; Gerber, C. *Adv. Mater.* **1996**, *8*, 719.
(52) Delamarche, E.; Michel, B. *Thin Solid Films* **1996**, *273*, 54.
(53) Haussling, L.; Michel, B.; Ringsdorf, H.; Rohrer, H. *Angew. Chem., Int. Ed. Engl.* **1991**, *30*, 569.
(54) Mizutani, W.; Michel, B.; Schierle, R.; Wolf, H.; Rohrer, H. *Appl. Phys. Lett.* **1993**, *63*, 147.
(55) Mizutani, W.; Anselmetti, D.; Michel, B. In *Local Probe Investigation of Self-Assembled Monolayers*; Blochl, P. E., Eds.; Kluwer Academic: The Netherlands, 1993; p 43.
(56) Durig, U.; Zuger, O.; Michel, B.; Haussling, L.; Ringsdorf, H. *Phys. Rev. B.* **1993**, *48*, 1711.
(57) Takami, T.; et al. *Langmuir* **1995**, *11*, 3876.
(58) Sprik, M.; et al. *Langmuir* **1994**, *10*, 4116.
(59) Nakamura, T.; Kondoh, H.; Matsumoto, M.; Nozoye, H. *Langmuir* **1996**, *12*, 5977.
(60) Mizutani, W.; Motomatsu, M.; Tokumoto, H. *Thin Solid Films* **1996**, *273*, 70.
(61) Li, W.; Virtanen, J. A.; Penner, R. M. *J. Phys. Chem.* **1994**, *98*, 11751.
(62) Li, W.; Virtanen, J. A.; Penner, R. M. *Langmuir* **1995**, *11*, 4361.
(63) Poirier, G. E.; Tarlov, M. J. *Langmuir* **1994**, *10*, 2853.
(64) Poirier, G. E.; Tarlov, M. J.; Rushmeier, H. E. *Langmuir* **1994**, *10*, 3383.
(65) Poirier, G. E.; Tarlov, M. J. *J. Phys. Chem.* **1995**, *99*, 10966.
(66) Poirier, G. E.; Pylant, E. D.; White, J. M. *J. Chem. Phys.* **1996**, *105*, 2089.
(67) Poirier, G. E.; Pylant, E. D. *Science* **1996**, *272*, 1145.
(68) Poirier, G. E. *J. Vac. Sci. Technol. B* **1996**, *14*, 1453.
(69) Poirier, G. E. *Langmuir* **1997**, *13*, 2019.
(70) Camillone, N.; et al. *J. Chem. Phys.* **1994**, *101*, 11031.
(71) Aviram, A.; Joachim, C.; Pomerantz, M. *Chem. Phys. Lett.* **1988**, *146*, 490.
(72) McDermott, C. A.; McDermott, M. T.; Green, J. B.; Porter, M. D. *J. Phys. Chem.* **1995**, *99*, 13257.
(73) Widrig, C. A.; Alves, C. A.; Porter, M. D. *J. Am. Chem. Soc.* **1991**, *113*, 2805.
(74) Boland, T.; Ratner, B. D. *Proc. Natl. Acad. Sci. USA* **1995**, *92*, 5297.
(75) Kang, J.; Rowntree, P. A. *Langmuir* **1996**, *12*, 2813.
(76) Truong, K. D.; Rowntree, P. A. *Prog. Surf. Sci.* **1995**, *50*, 207.
(77) Sondag-Huethorst, J. A. M.; Shonenberger, C.; Fokkink, L. G. J. *J. Phys. Chem.* **1994**, *98*, 6826.
(78) Schonenberger, C.; Sondag-Huethorst, J. A. M.; Jorritsma, J.; Fokkink, L. G. J. *Langmuir* **1994**, *10*, 611.
(79) Schonenberger, C.; Jorritsma, J.; Sondag-Huethorst, J. A. M.; Fokkink, L. G. J. *J. Phys. Chem.* **1995**, *99*, 3259.
(80) Dhirani, A.-A.; Zehner, R. W.; Hsung, R. P.; Guyot-Sionnest, P.; Sita, L. R. *J. Am. Chem. Soc.* **1996**, *118*, 3319.
(81) Dhirani, A.; Lin, P.-H.; Guyot-Sionnest, P.; Zehner, R. W.; Sita, L. R. *J. Chem. Phys.* **1997**, *106*, 5249.
(82) Rohwerder, M.; Weldige, K. d.; Vago, E.; Viefhaus, H.; Stratmann, M. *Thin Solid Films* **1995**, *264*, 240.

(83) Stranick, S. J.; Weiss, P. S.; Parikh, A. N.; Allara, D. L. *J. Vac. Sci. Technol. A.* **1993**, *11*, 739.
(84) Stranick, S. J.; Parikh, A. N.; Allara, D. L.; Weiss, P. S. *J. Phys. Chem.* **1994**, *98*, 11136.
(85) Stranick, S. J.; Parikh, A. N.; Tao, Y.; Allara, D. L.; Weiss, P. S. *J. Phys. Chem.* **1994**, *98*, 7636.
(86) Stranick, S. J.; et al. *J. Vac. Sci. Technol. B* **1994**, *12*, 2004.
(87) Stranick, S. J.; et al. *Nanotechnology* **1996**, *7*, 438.
(88) Bumm, L. A.; et al. *Science* **1996**, *271*, 1705.
(89) Weiss, P. S.; et al. *Anal. Chim. Acta* **1995**, *307*, 355.
(90) Chidsey, C. E. D.; Loiacono, D. N.; Sleator, T.; Nakahara, S. *Surf. Sci.* **1988**, *200*, 45.
(91) Sandy, A. R.; Mochrie, S. G. J.; Zehner, D. M.; Huang, K. G.; Gibbs, D. *Phys. Rev. B* **1991**, *43*, 4667.
(92) Woll, C.; Chiang, S.; Wilson, R. J.; Lippel, P. H. *Phys. Rev. B* **1989**, *39*, 7988.
(93) Chambliss, D. D.; Wilson, R. J.; Chiang, S. *J. Vac. Sci. Technol. B* **1991**, *9*, 933.
(94) Strong, L.; Whitesides, G. M. *Langmuir* **1988**, *4*, 546.
(95) Chidsey, C. E. D.; Loiacono, D. N. *Langmuir* **1990**, *6*, 682.
(96) Nuzzo, R. G.; Korenic, E. M.; Dubois, L. H. *J. Chem. Phys.* **1990**, *93*, 767.
(97) Camillone, N.; Chidsey, C. E. D.; Liu, G.-y.; Scoles, G. *J. Chem. Phys.* **1993**, *98*, 3503.
(98) Fenter, P.; Eisenberger, P.; Liang, K. S. *Phys. Rev. Lett.* **1993**, *70*, 2447.
(99) Fenter, P.; Eberhardt, A.; Eisenberger, P. *Science* **1994**, *266*, 1216.
(100) Villarrubia, J. S. *Surf. Sci.* **1994**, *321*, 287.
(101) Mar, W.; Klein, M. L. *Langmuir* **1994**, *10*, 188.
(102) Yeganeh, M. S.; Dougal, S. M.; Polizzotti, R. S.; Rabinowitz, P. *Phys. Rev. Lett.* **1995**, *74*, 1811.
(103) Camillone, N.; et al. *J. Chem. Phys.* **1993**, *99*, 744.
(104) Bain, C. D.; Biebuyck, H. A.; Whitesides, G. M. *Langmuir* **1989**, *5*, 723.
(105) Olbris, D. J.; Ulman, A.; Shnidman, Y. *J. Phys. Chem.* **1995**, *102*, 6865.
(106) Sun, L.; Johnson, B.; Wade, T.; Crooks, R. M. *J. Phys. Chem.* **1990**, *94*, 8869.
(107) Nishikata, Y.; Kakimoto, M.-A.; Morikawa, A.; Imai, Y. *Thin Solid Films* **1988**, *160*, 15.
(108) Hautman, J.; Klein, M. *Phys. Rev. Lett.* **1991**, *67*, 1763.
(109) Miller, C.; Cuendet, P.; Gratzel, M. *J. Phys. Chem.* **1991**, *95*, 877.
(110) Nuzzo, R. G.; Dubois, L. H.; Allara, D. L. *J. Am. Chem. Soc.* **1990**, *112*, 558.
(111) Bain, C. D., et al. *J. Am. Chem. Soc.* **1989**, *111*, 321.
(112) Bain, C. D.; Whitesides, G. M. *J. Am. Chem. Soc.* **1989**, *111*, 7164.
(113) Thomas, R. C.; Sun, L.; Crooks, R. M.; Ricco, A. J. *Langmuir* **1991**, *7*, 620.
(114) Buck, M.; Grunze, M.; Eisert, F.; Fischer, J.; Trager, F. *J. Vac. Sci. Technol. A* **1992**, *10*, 926.
(115) Karpovich, D. S.; Blanchard, G. J. *Langmuir* **1994**, *10*, 3315.
(116) Camillone, N.; Leung, T. Y. B.; Schwartz, P.; Eisenberger, P.; Scoles, G. *Langmuir* **1996**, *12*, 2737.
(117) Allen, S. M.; Cahn, J. W. *Acta Metall.* **1979**, *27*, 1085.
(118) Stroscio, J. A.; Pierce, D. T.; Dragoset, R. A.; First, P. N. *J. Vac. Sci. Technol. A* **1992**, *10*, 1981.